ENVIRONMENTAL RESEARCH
COMMUNICATIONS

INCLUSIVE PUBLISHING
TRUSTED SCIENCE

Part of the
ENVIRONMENTAL RESEARCH
SERIES

PURPOSE-LED
PUBLISHING™

**LETTER** • **OPEN ACCESS**

# Eddy-topography interactions drive ocean ventilation across the Eocene–Oligocene transition: insights from a hierarchy of ocean model simulations

To cite this article: A Klocker *et al* 2026 *Environ. Res. Commun.* **8** 051015

Environmental Research Communications



OPEN ACCESS

RECEIVED
16 October 2025

REVISED
21 April 2026

ACCEPTED FOR PUBLICATION
5 May 2026

PUBLISHED
15 May 2026



LETTER

# Eddy-topography interactions drive ocean ventilation across the Eocene–Oligocene transition: insights from a hierarchy of ocean model simulations

**A Klocker**[1,*], **P E Isachsen**[2,3], **D R Munday**[4], **I Sauermilch**[5,6] **and J M Whittaker**[5]

[1] NORCE Research AS, Bjerknes Centre for Climate Research, Bergen, Norway
[2] Department of Geosciences, University of Oslo, Oslo, Norway
[3] Section for Ocean and Ice, Norwegian Meteorological Institute, Oslo, Norway
[4] British Antarctic Survey, Cambridge, United Kingdom
[5] Institute for Marine and Antarctic Studies, University of Tasmania, Hobart, Australia
[6] Department of Earth Sciences, Faculty of Geosciences, Utrecht University, Utrecht, The Netherlands
[*] Author to whom any correspondence should be addressed.

**E-mail:** ankl@norceresearch.no

**Keywords:** climate modelling, subgrid-scale parameterisations, ocean circulation, Eocene–Oligocene transition

## Abstract

The Eocene–Oligocene transition (EOT), approximately 34 million years ago, represents one of the most profound climate shifts in Earth's history—a rapid cooling that marked the transition from the warm Eocene greenhouse to the Cenozoic icehouse. The mechanisms driving this transition remain debated: proposed causes include a decline in atmospheric $CO_2$ concentrations and tectonic opening of Southern Ocean gateways, namely Drake Passage and the Tasman Gateway, which altered ocean circulation and poleward heat transport. Here we use ocean model simulations spanning a wide range of spatial resolutions—from a coarse-resolution, eddy-parameterised configuration to high-resolution, eddy-resolving simulations—to investigate how the representation of ocean eddies affects the simulated circulation response to gateway opening. Our results show that the establishment of a proto Antarctic Circumpolar Current (ACC), even if much weaker than today's current, led to the onset of coastal upwelling along the Antarctic continental slope in the Australian Antarctic Basin (AAB). This upwelling has previously been linked to the onset of biogenic blooms and associated carbon drawdown in the Southern Ocean. The simulations suggest that the proto-ACC followed the Antarctic continental slope in the AAB and that upwelling was driven by either bottom Ekman transport beneath this slope current or, as indicated by the highest-resolution simulations, eddy-topography interactions—a process in which mesoscale eddies interacting with rough and steeply sloping bottom topography drive a net onshore transport of dense waters. Critically, neither a distinct continental slope current nor the associated upwelling is reproduced in coarse-resolution models using existing eddy parameterisations, implying that the climatic impact of Southern Ocean gateway opening during the EOT has been substantially underestimated in previous modelling studies.

## 1. Introduction

Earth system models (ESMs) are essential tools for understanding past and future climates, but computational constraints often require coarse grid spacing, particularly for paleoclimate applications requiring extended simulations. Hence, there are important subgrid-scale and therefore unresolved processes which must be parameterised in ESMs using simplified mathematical formulations to replicate their net effects on the resolved large-scale fields.

Ocean mesoscale eddies exemplify such subgrid-scale processes. These 10–100 km structures, with lifetimes from days to a year [1, 2], profoundly influence large-scale ocean circulation and climate by stirring and transporting water properties like temperature, salinity and momentum, as well as tracers

like carbon [3–5]. While current ESMs are beginning to resolve eddies, they remain rare in paleoclimate models. Here, we use ocean simulations spanning eddy-parameterised to eddy-resolving grid resolutions to assess how well parameterisations capture eddies' net effects on large-scale flow, using the Eocene–Oligocene transition (EOT) as our test case.

The EOT (∼34 million years ago) marked an abrupt climate cooling (∼2.9 °C [6]) that bridged the Eocene greenhouse and Cenozoic icehouse [7, 8]. This transition involved dramatic declines in global and deep ocean temperatures [9, 10] and expansion of Antarctic glaciation [11, 12]. Two primary driving mechanisms are debated: declining atmospheric $CO_2$ [11–13], and the onset of a thermally-insulating Antarctic Circumpolar Current (ACC) following tectonic opening of Drake Passage and Tasman Gateway (DP and TG in the following) [14, 15]. Both proposals face challenges: the $CO_2$ mechanism lacks a clear carbon sink [16–18], while the ACC likely achieved significant strength only in the late Miocene, ∼20 million years later [19]. Recent work suggests northern high-latitude gateway changes may also have contributed [20–22], though no consensus exists on the relative roles of southern versus northern processes.

The picture has been substantially revised by a new generation of Southern Hemisphere eddy-permitting and eddy-resolving simulations [7, 18, 23, 24], combined with improved paleobathymetric reconstructions [25]. The simulations by Sauermilch *et al* [7] reveal that large-scale gyres in the Southern Ocean's Pacific and Atlantic sectors are considerably stronger when eddies are resolved, consistent with results from idealised models [26], and that gateway deepening triggers strong Antarctic coastal cooling through the weakening of these gyres. According to the authors, the coastal cooling was therefore not primarily due to the development of a thermally-insulating 'proto-ACC' since this circumpolar current after gateway deepening was still only 10%–20% of its modern-day strength. Furthermore, very high-resolution and fully eddy-resolving simulations studied by Hochmuth *et al* [18] of the Australian Antarctic Basin (AAB) are consistent with an observed package of biogenic sediment whose accumulation in this basin is also attributed to gateway opening. More specifically, this work showed that gateway deepening led to the development of an eastward-flowing current along the Antarctic continental slope in the AAB and that Ekman upwelling underneath this current, bringing nutrient-rich water to the surface, was a key ingredient for the sediment deposition. This sediment package may represent the 'missing carbon' sequestered during the Eocene-to-Oligocene $CO_2$ decline, providing a direct mechanistic link between ocean circulation changes and atmospheric $CO_2$ drawdown across the EOT. Crucially, none of these circulation changes are reproduced in coarse-resolution simulations where eddies are parameterised rather than resolved.

A key conclusion made by Sauermilch *et al* [7] was that a correct representation of Southern Ocean gyre weakening, reduced heat transport and cooling along the Antarctic coast, required high enough model resolution that ocean eddies were at least partially resolved. Hochmuth *et al* [18] did not examine the sensitivity to model resolution and the role of ocean eddies on the upwelling that led to biogenic sedimentation in the AAB. The question emerges whether present-day coarse-grained climate models, using parameterised ocean eddies, are capable to reproduce this possibly very important event in Earth's history. Examining this question is the central focus of the present study. To do so we re-analyse a subset of the model simulations from [7] and [18]. The new analysis shows that the development of the coastal current in the AAB, most likely a branch of the circumpolar proto-ACC, also requires eddy-permitting model resolution. The vertical structure and upwelling associated with this current is also resolution-dependent, suggesting that eddy processes are at play. We then argue for why the eddy parameterisations most commonly used in modern ESMs are fundamentally unable to represent the dynamics sustaining this upwelling, and discuss the implications for previous coarse-resolution modelling studies of the EOT. Finally, we outline pathways forward through both improved parameterisations and the development of computationally efficient eddying ESMs that could make eddy-resolving paleoclimate simulations feasible in the near future.

## 2. Model configurations

The simulations are carried out with the Massachusetts Institute of Technology general circulation model (MITgcm [27]) in an ocean-only configuration without sea ice (it is expected that during the EOT sea surface temperatures were too high for sea ice to form). This allows for a focus on the representation of ocean eddies and bathymetric detail on ocean circulation without the added complexity of a fully-coupled ESM. The grid spacing ranges from 1° (eddies parameterised), to 1/4° (eddies partially resolved), 1/10° (eddies largely resolved) and 1/40° (mesoscale eddies fully resolved and smaller 'submesoscale' eddies partially resolved). Due to computational constraints we use a circumpolar

**Table 1.** Model simulations used in this study. 'Domain' refers to the model domains, whether circumpolar or focused on the Australian Antarctic Basin. 'Gateway' refers to the depth of the Tasman Gateway (TG). 'Grid' refers to the grid spacing. 'Eddy' refers to the representation of ocean eddies, where 'GM' is using the eddy parameterisation by [28], whereas 'none' means that no eddy parameterisation is used. 'Spinup' refers to the spinup time used to get the model simulation to quasi-equilibrium, and 'vert. levels' refers to the vertical levels used in the model configurations.

| Model simulations | | | | | | |
|---|---|---|---|---|---|---|
| Simulation name | Domain | Gateway | Grid | Eddy | Spinup | vert. levels |
| TG300_1° | Circumpolar | 300 m | 1° | GM90 | 110 yrs | 50 |
| TG1500_1° | Circumpolar | 1500 m | 1° | GM90 | 110 yrs | 50 |
| TG0_1/4° | Circumpolar | 0 m | 1/4° | none | 110 yrs | 50 |
| TG300_1/4° | Circumpolar | 300 m | 1/4° | none | 110 yrs | 50 |
| TG450_1/4° | Circumpolar | 450 m | 1/4° | none | 110 yrs | 50 |
| TG600_1/4° | Circumpolar | 600 m | 1/4° | none | 110 yrs | 50 |
| TG1500_1/4° | Circumpolar | 1500 m | 1/4° | none | 110 yrs | 50 |
| TG300_1/10° | Aus. Ant. basin | 300 m | 1/10° | none | 8 yrs | 150 |
| TG1500_1/10° | Aus. Ant. basin | 1500 m | 1/10° | none | 8 yrs | 150 |
| TG0_1/40° | Aus. Ant. basin | 0 m | 1/40° | none | 8 yrs | 150 |
| TG300_1/40° | Aus. Ant. basin | 300 m | 1/40° | none | 8 yrs | 150 |
| TG450_1/40° | Aus. Ant. basin | 450 m | 1/40° | none | 8 yrs | 150 |
| TG600_1/40° | Aus. Ant. basin | 600 m | 1/40° | none | 8 yrs | 150 |
| TG1500_1/40° | Aus. Ant. basin | 1500 m | 1/40° | none | 8 yrs | 150 |

domain for the coarser-resolution simulations (1°, 1/4°), and a regional domain, focusing on the AAB, for the higher-resolution simulations (1/10°, 1/40°). For a grid spacing of 1°, eddies are parameterised using the widely-used Gent-McWilliams (GM) eddy parameterisation [28, 29] using a coefficient of $\kappa = 1000\,\mathrm{m^2\,s^{-1}}$, whereas for all other grid spacings no eddy parameterisation is used. Note here that the grid spacing of 1° is what is most often used in current ESMs, with some using a grid spacing of 1/4°, and only the most cutting-edge ESM simulations using a grid spacing of 1/10°. We use the paleobathymetry of [25] for all simulations.

For the 1/4° grid spacing we compare simulations where the Tasman Gateway (TG) is progressively widened and deepened, with the deepest point increasing from 0 m to 300 m, 450 m, 600 m and 1500 m (see figure 1 and supplementary figure 10 in [7] for a detailed illustration of the TG bathymetry at different depths), while leaving the deepest point in Drake Passage at 1000 m (results are very similar for the deepening of Drake Passage while leaving the depth of TG constant; see [7]). As the gateway deepens, its width also increases substantially—from an essentially closed configuration with a chain of islands breaching the sea surface, to a broad open passage. The stated gateway depth throughout this manuscript refers to the deepest point across the TG; significant bathymetry shallower than this value is present across the gateway, particularly at the shallowest configurations. It is therefore the combination of gateway width and depth that governs whether ambient potential vorticity (PV) contours are blocked by the Antarctic continent or wrap around it to facilitate a circumpolar flow mode. For other grid spacings we run simulations with a TG of 300 m and 1500 m, which, as shown by [18], cover the most dominant change across the EOT and can be compared to the results by [7].

All model simulations are summed up in table 1. The circumpolar model domain covers the entire Southern Ocean, extending from 84°S to 25°S. We use 50 vertical layers, ranging from 10 m at the surface to 368 m at the bottom. Surface forcing (i.e. sea surface temperature, sea surface salinity and wind stress) are zonal and temporal means taken from a coupled atmosphere-ocean model (GFDL CM2.1) simulating Late Eocene conditions with atmospheric $CO_2$ concentrations of 800ppm [30].

The regional domain, focusing on the AAB, is one-way nested within the circumpolar domain and extends from 100°E to 165°E in zonal direction and from 65°S to 49°S in meridional direction. These configurations are run at an eddying grid spacing of 1/10° and a submesoscale-permitting grid spacing of 1/40°, both with 150 levels in the vertical, ranging from 10 m at the surface to 50 m at the bottom. These model simulations are the same as used by [18].

The simulations have been spun up for 110 years for the circumpolar domain, and 8 years for the AAB domain, resulting in near-equilibrium. More detail about these simulations can be found in [7, 23], and [18].

## 3. Circumpolar flow changes due to gateway deepening

Figure 1 shows sea surface height (SSH) from the 1/4° simulation for a TG depth of (a) 300 m and (b) 1500 m, with (c) showing the difference. For a TG depth of 300 m, SSH shows a pronounced minimum in the centre of gyres located in the Pacific and Atlantic sectors, and maxima both towards the northern boundary and the Antarctic coast. The gyres are still dominating features for a TG depth of 1500 m, although they are weakened, as pointed to by Sauermilch *et al* [7]. More notably, SSH along the Antarctic coast becomes around half a meter lower after TG opening. This is, by geostrophic balance, associated with eastward currents. In the Pacific sector the SSH drop is largely associated with a counter-clockwise gyre in the Ross Sea. But elsewhere, and particularly in the AAB where the signal is the strongest, the drop is associated with circumpolar throughflow, that is a near-coastal branch of the proto-ACC which strengthened after gateway deepening.

The eastward direction of the simulated slope current contrasts with the modern westward Antarctic Slope Current (ASC), but this is physically expected. The modern ASC is linked to the Antarctic Slope Front—a cross-slope density gradient generated by ocean–sea-ice and ocean–ice-shelf interactions [31]. In the Late Eocene, sea surface temperatures were considerably warmer and sea ice and ice shelf extent were likely much reduced, weakening or eliminating this buoyancy forcing. The simulated eastward slope current in the AAB is therefore best understood as a branch of the large-scale proto-ACC steered onto the continental slope by the ambient PV structure following gateway deepening, rather than a locally buoyancy-driven current like the modern ASC.

The temperature change at 100 m depth for the same simulations are shown in figures 1(d)–(f). As with SSH, the largest changes are found along the Antarctic coast, with a cooling of up to 5 °C. Over most of the domain, this cooling after TG deepening is partially due to weakening of the subpolar gyres, which bring heat to the Antarctic continent [7]. But in the AAB, where the temperature drop is also largest, it is instead due to a sudden onset of coastal upwelling which brings cold waters to the surface [18]. Note that these changes occur in a one-off reorganisation of ocean currents once TG deepens from 300 m to 450 m, as shown by [18]. Throughout this manuscript, we use the terms 'abrupt' and 'sudden onset' to describe this highly nonlinear sensitivity of ocean circulation to gateway depth—that is, a large change in circulation response for a relatively small additional increase in TG depth—rather than to imply any temporal suddenness, since all simulations presented here are time-averaged fields from equilibrated model runs. In the following we use the fields for TG depths of 300 m and 1500 m to highlight ocean states either side of this reorganisation since these simulations exist for all resolutions.

Figure 2 shows the same two fields, SSH and temperature at 100 m depth, for the low-resolution simulation with a grid spacing of 1° and parameterised eddy transport. For shallow gateway depth, the gyres in these low-resolution simulations are much weaker than in the eddy-permitting 1/4° model [7]. In addition, they all but vanish after gateway opening, leading instead to a broad sea level drop from north to south, that is, a broad circumpolar proto-ACC—but with a transport of only 7%–19% of today's net transport [7]. There is also a weak temperature drop along the Antarctic coast, but this too is a much broader feature than in the eddy-permitting simulation. So, whilst the changes after gateway opening are superficially the same between the two resolutions, the eddy-permitting model produces a stronger and more latitudinally confined SSH change, representative of a coastally-trapped flow, and a longitudinally elongated temperature change of much greater magnitude than the low-resolution model.

## 4. Flow changes and upwelling in the AAB

We now zoom in on the AAB (the region is highlighted by a cyan box in figure 1(a) to further examine the development of the eastward current along the Antarctic continental slope and its possible role in enhanced upwelling along the coast. To this end, we compare runs for gateway depths of 300 m and 1500 m for grid spacings of 1°, 1/4°, 1/10°, and 1/40°.

Figure 3 shows zonal velocity in the AAB, both at 100 m depth and as a function of depth through a representative north-south transect. In the 1° simulation, there is a broad and, as seen here, very 'baroclinic' and surface-intensified ACC-like eastward flow for both gateway depths. Deepening of the TG has little effect beyond a modest strengthening of this broad current. In contrast, all the higher-resolution simulations show a series of zonal jets across the AAB—for both 300 m and 1500 m gateway depths. These jets manifest as distinct bands that tend to be 'barotropic', that is extending throughout the entire water column. They also predominately flow along steep topographic features, reflecting steering by the

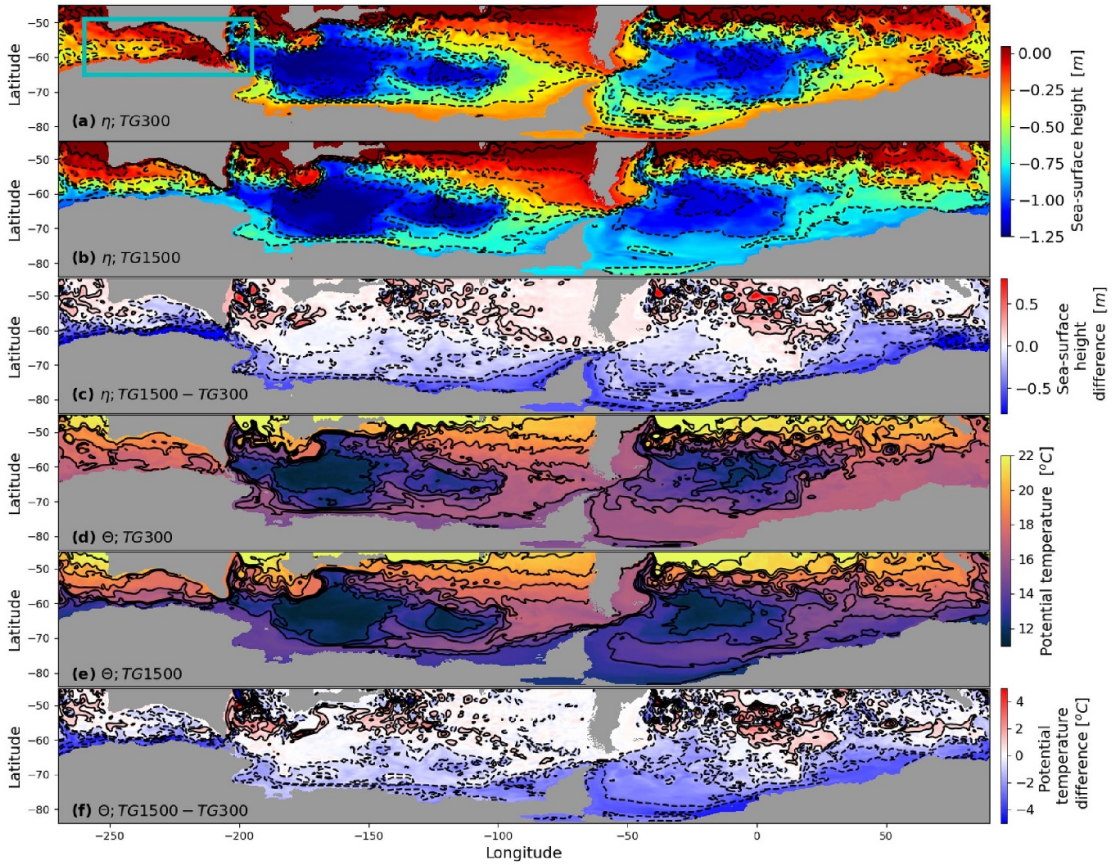


**Figure 1.** Sea-surface height and potential temperature for eddying experiments. (a), (b) Mean sea-surface height, and (d), (e) potential temperatures at 100 m depth, are shown for the eddying simulations with a grid spacing of 1/4° for a TG depth of (a), (d) 300 m and (b), (e) 1500 m. Differences for a TG deepening from 300 m to 1500 m are shown for (c) mean sea-surface height and (f) potential temperatures at 100 m. The cyan rectangle in (a) shows the AAB high-resolution model domain.

topographic PV gradient [32]. But, notably, the jets are narrower than the topographic features themselves. This suggests some level of jet sharpening facilitated by up-gradient lateral eddy momentum fluxes [33].

In the higher-resolution simulations, the main difference introduced by the actual gateway deepening is the appearance of the eastward current on the upper Antarctic continental slope, around 60° S. Before deepening, the basin circulation is dominated by a clockwise gyre, giving westward flow near the slope. This gyre is then pushed northward as the eastward current emerges. The current follows the slope throughout the AAB but then leaves the coast at the topographic saddle point of the TG and continues into the Pacific sector along the east coast of Australia. We take this as indication that this 'slope current' in the AAB is a branch of the proto-ACC which meanders its way around the entire Southern Ocean, as also suggested by Hochmuth *et al* [18].

The passive tracer fields shown in figures 3(q) and (r) for the 1/40° 1500 m gateway simulation illustrate the two key components of the ocean circulation that together drive the biogenic sediment accumulation documented by Hochmuth *et al* [18]. The first tracer, injected in the surface layer in the northwest corner of the domain, traces the clockwise gyre circulation that brings warm, nutrient-rich waters from mid-latitudes towards the Antarctic coast. The second tracer, injected at depths of ∼300–500 m where salinity exceeds 34.7 psu, illustrates the upwelling of dense subsurface waters along the continental slope. It is the combination of these two circulation features—the gyre-driven supply of nutrients and the slope-current-driven upwelling of deep waters—that Hochmuth *et al* [18] propose drove the onset of biogenic blooms and the subsequent sequestration of carbon in the sediment record across the EOT. Neither of these features is present in the 1° eddy-parameterised simulation (not shown), underscoring the climatic importance of correctly representing the circulation changes discussed here.

To examine the relationship between the slope current and upwelling, zonal velocities and isopycnals (iso-surfaces of constant potential density) in the upper 750 m along the AAB transect are plotted in figure 4. The fields here are taken from the 1/40° simulation and clearly reveal that the establishment of the slope current takes place as TG depth transitions from 300 m to 450 m. This current, or more

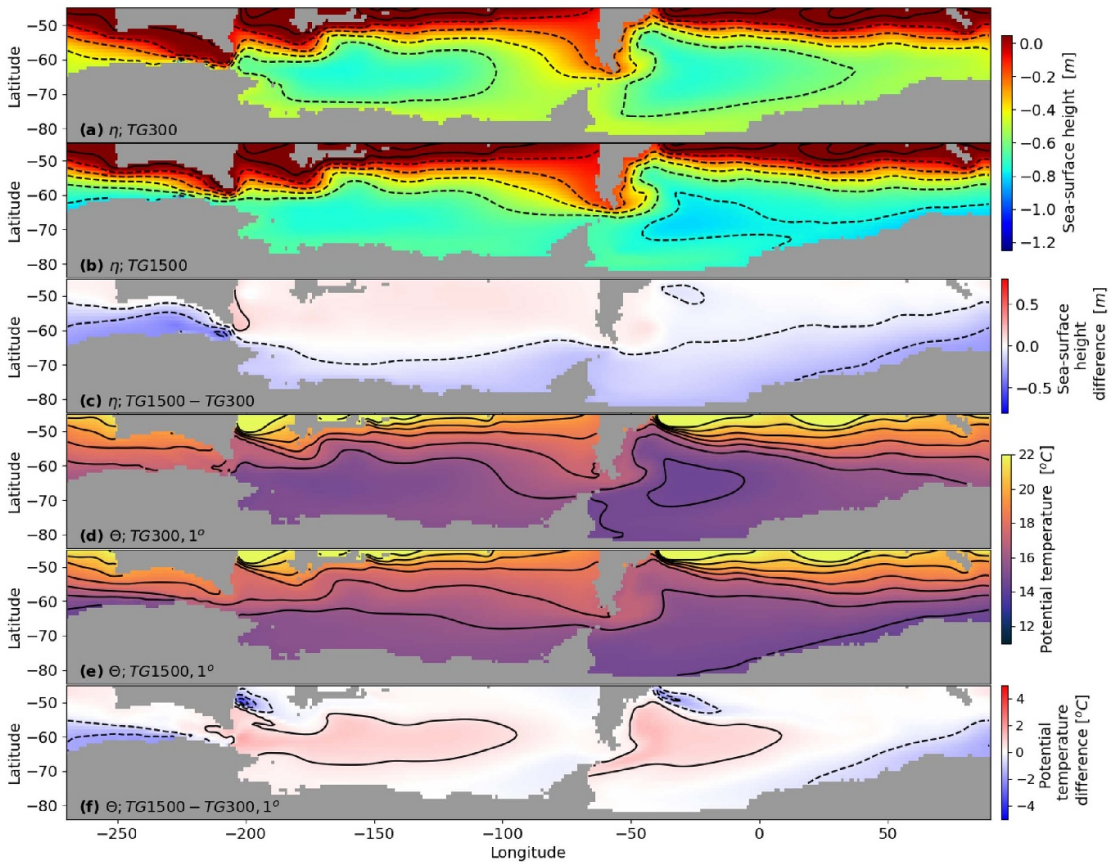


**Figure 2.** Sea-surface height and potential temperature for eddy-parameterised experiments. Same as figure 1, but for the eddy-parameterised simulations with a grid spacing of 1°.

specifically its vertical shear, is associated, through the thermal wind balance, with a distinct lifting of isopycnals over the continental slope, indicating upwelling of dense waters towards the surface.

The full progression in figure 4 is instructive. For a closed TG, isopycnals tilt downward toward the coast, consistent with gyre-driven downwelling. At a TG depth of 300 m this weakens but the slope current has not yet established, producing neither strong downwelling nor upwelling. The transition to upwelling at a TG depth of 450 m coincides with the onset of the slope current and, as discussed in the next section, a strong lateral shear between the eastward slope current and the westward offshore flow.

Germane to our focus here, upwelling over the Antarctic continental slope is very weak in the 1° simulation where a distinct slope current does not develop. So the slope current is key. But with this current established in the higher-resolution simulations, what processes are responsible for upwelling of cold deep waters? In the 1/4° simulation the slope current is deep-reaching and extends to the bottom (figure 3). So here a plausible source of coastal upwelling is bottom Ekman transport, which for an eastward-flowing current in the southern hemisphere is directed southwards and, here, up the continental slope [18]. However, at even higher model resolution, especially at 1/40°, the slope current has a much higher vertical shear and is actually quite weak at the bottom. It is therefore questionable whether bottom Ekman transport can be responsible for much of the coastal upwelling in this simulation. As indicated in figure 5, isopycnal slopes over the continental slope are resolution-dependent, and actual surface outcropping of deep isopycnals over the slope generally enhances as resolution increases. This behaviour, which is also seen in other transects cutting through the AAB (not shown), suggests that eddy motions, best resolved in the 1/40° simulation, contribute to upwelling. The next section looks into the relevant dynamics in more detail and points to why the current GM eddy parametrisation scheme, used in the 1° simulation, will fail at reproducing any eddy-driven upwelling—and will reduce upwelling caused by any other process, for example by bottom Ekman transport.

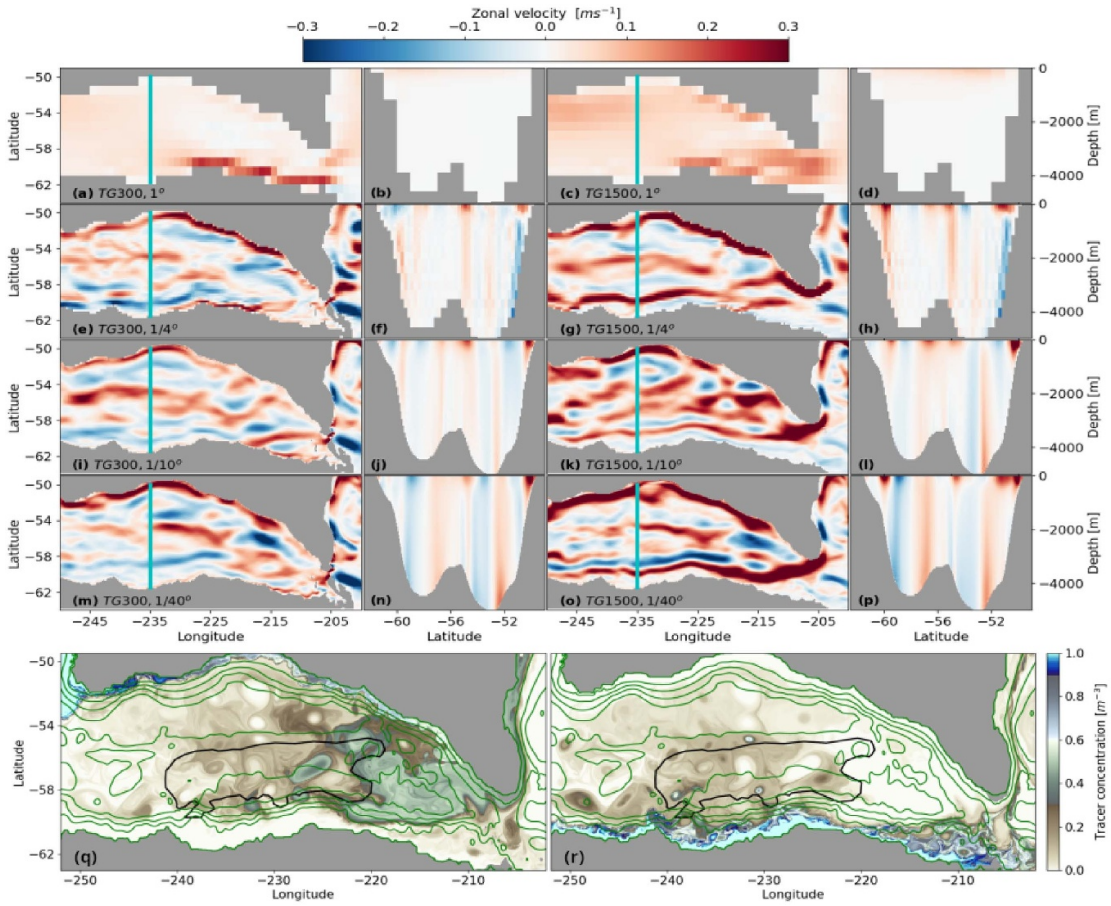


**Figure 3.** Zonal velocities and passive tracer. Mean zonal velocities are shown for (a), (c), (e), (g), (i), (k), (m), (o) a horizontal section at 100 m depth and (b), (d), (f), (h), (j), (l), (n), (p) vertical sections shown by cyan lines in the latter. Simulations are shown for a grid spacing of (a)–(d) 1°, (e)–(h) 1/4°, (i)–(l) 1/10°, and (m)–(p) 1/40°. For the 1/40° 1500 m gateway simulation, passive tracers are shown injected (q) in the surface layer in the north-west corner of the domain, and (r) everywhere where salinity is greater than 34.7 psu, which equates to a depth range of ∼300–500 m. In the latter two panels, green contours represent bathymetry, and the black contour represents the outline of the sediment accumulation as estimated by [18].

## 5. Limitations of the GM eddy parameterisation

The most common source of eddies in the ocean is 'baroclinic' instability [34]. The central idea is that large-scale wind or buoyancy forcing steepens isopycnals in the ocean until the flow becomes unstable and small perturbations can grow explosively. Eddies are generated by this instability, fuelled by the extraction of potential energy and its conversion to kinetic energy, as they work to flatten the same isopycnals. In an equilibrated state the steepness of isopycnals will reflect a balance between the large-scale forcing steepening them and the eddies flattening them [35]. The GM eddy parameterisation scheme, used in most ESMs and also in our 1° simulation, is designed with this in mind, setting up an eddy-induced transport velocity that flattens isopycnals [28, 29]. If the forcing is taken away, the GM scheme flattens the isopycnals until they become horizontal.

Potential energy release by baroclinic instability is certainly taking place in all eddy-permitting simulations studied here. However, it is also apparent from figures 4 and 5 that ocean dynamics that are only present at high resolution steepen rather than flatten isopycnals over the Antarctic continental slope in the AAB as the slope current is established. As outlined above, some of the upwelling may be associated with flow towards the coast in a bottom Ekman layer below the emerging coastal current. But the slope current is quite weak at the bottom in the highest-resolution simulation and figure 5 also indicates that the upwelling strengthens as model resolution increases, pointing to an important role for smaller-scale eddy or wave motions.

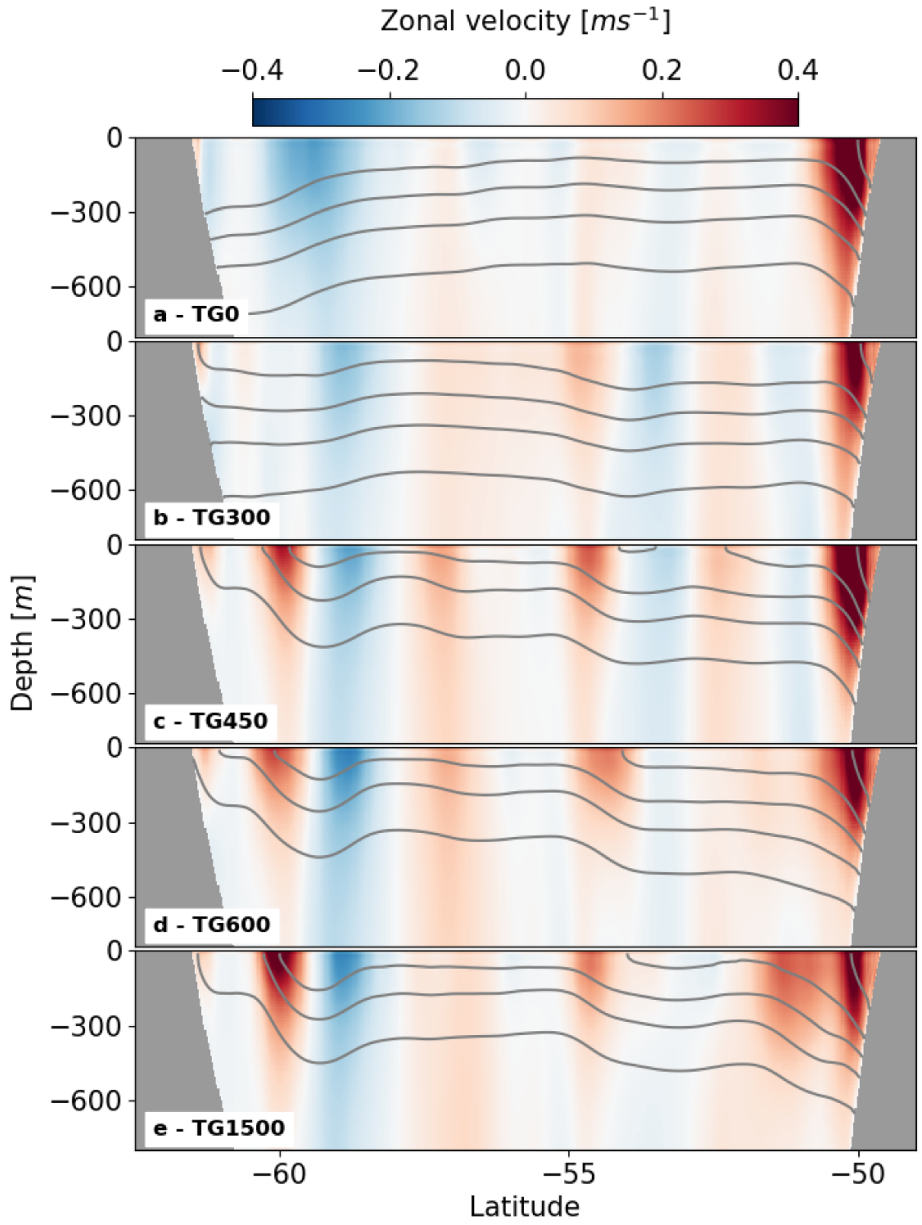


**Figure 4.** Zonal velocities and isopycnals for 1/40° grid spacing. Mean zonal velocities (shading) and isopycnals (grey contours) are shown for the top 750 m of the water column for the 1/40° grid spacing experiments along the sections shown by the cyan line in figure 3 for a TG depth of (a) 0 m, (b) 300 m, (c) 450 m, (d) 600 m, and (e) 1500 m. Note that these panels appear as supplementary figure 8 in Hochmuth *et al* [18], where they were presented as context for interpreting the sediment accumulation record rather than as the focus of dynamical analysis.

Two related processes may be at play. The first relies on the fact that mesoscale eddies stir and transport PV, a combination of water column spin and thickness. Over a flat bottom the eddies produced by baroclinic instability will transport thickness in such a way as to flatten isopycnals—in line with GM. But over a *corrugated* continental slope (the corrugations reflecting e.g. submarine canyons) large and deep eddies will typically drive a net mass transport towards the coast, through the 'valleys' in the corrugations. This mass transport also contains the densest waters which are then deflected by the slope up towards the surface—the upwelling [36]. The question remains why there would be more eddies and eddy-driven upwelling over the Antarctic continental slope when the gateway deepens. The answer is most likely linked to the establishment of the slope current and, more specifically, to a strong horizontal velocity shear that develops between the slope current and a westward flowing current just offshore (figure 4). Such lateral current shear is prone to another type of instability, namely 'barotropic' instability in which eddies draw their energy from the large-scale kinetic energy of the two currents. Eddies formed by barotropic instability in this shear region can then interact with the corrugated continental slope, causing a PV flux and upwelling. So, while eddy motions and eddy-topography interactions

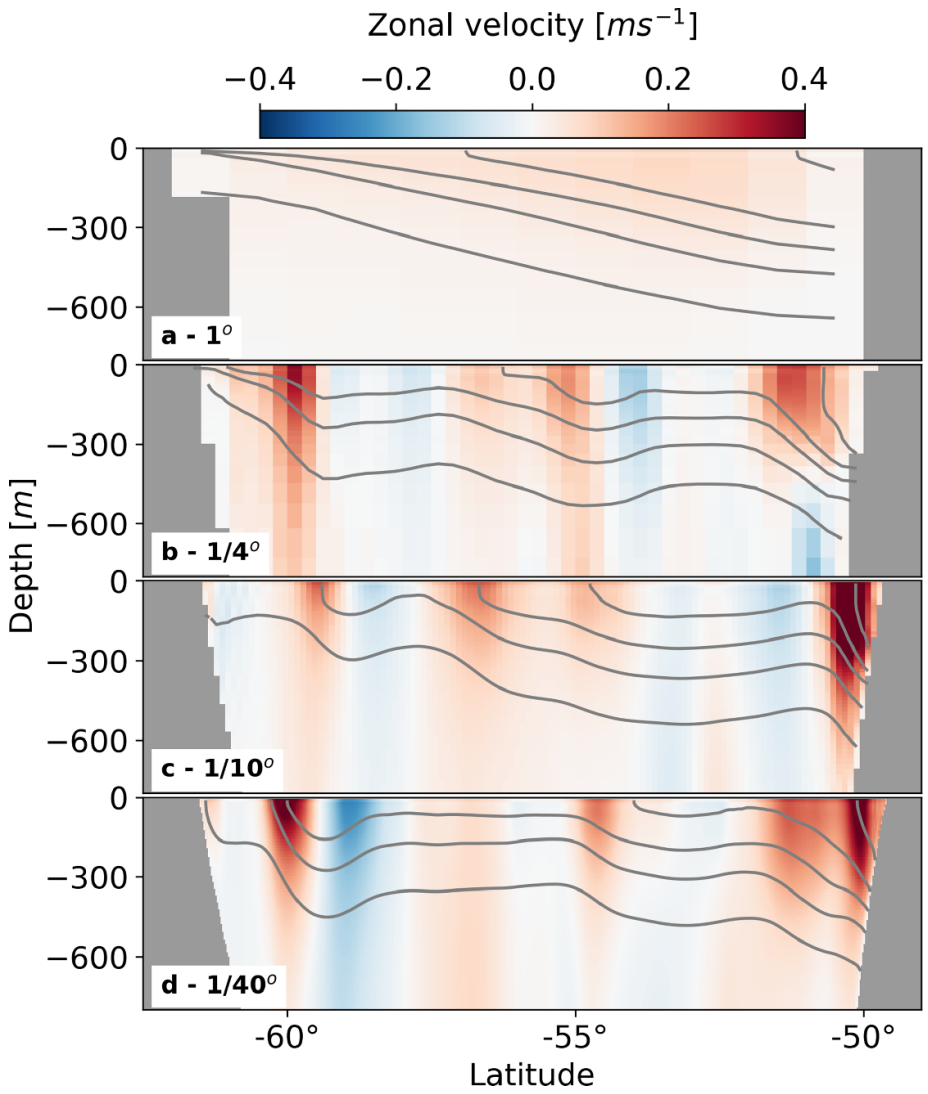


**Figure 5.** Zonal velocities and isopycnals for 1500 m gateway depth. Mean zonal velocities (shading) and isopycnals (grey contours) in the upper 750 m of the water column along the same transect as figure 4, shown for a TG depth of 1500 m across four model resolutions: (a) 1°, (b) 1/4°, (c) 1/10° and (d) 1/40°.

may be present at all gateway depths, what changes abruptly at a TG depth of 450 m is their intensity, amplified by barotropic instability of this shear zone.

Independent support for this interpretation comes from Klocker [37] and Bachman and Klocker [38], who used tracer release experiments in idealised settings with similar current configurations—specifically, the onset of strong lateral shear between an eastward slope current and a westward offshore current—to directly quantify the role of eddy-topography interactions in driving ocean ventilation. Those studies demonstrated that such lateral shear generates barotropic instability, producing eddies that interact with corrugated slope topography to drive strong ocean ventilation. The main difference between the jet dynamics explained by [37] and here is that in the former, the one-off reorganisation of ocean currents was triggered by an acceleration of the eastward jet due increasing winds, whereas here it is triggered by deepening of the TG. In both cases, it is the appearance of strong lateral shear between eastward and westward jets that leads to the onset of ocean ventilation.

Second, with the establishment of the slope current there is another process, related but not relying on eddies *per se*, that can also generate upwelling. The key point is that the slope current in the AAB at the time of the EOT flowed eastward, and this turns out to be in the opposite direction to the propagation of topographic waves along the slope. Such a current, when flowing against topographic waves over a corrugated bottom slope can generate large-amplitude arrested topographic waves when the flow speed is the same as the wave propagation speed—but oppositely directed [39, 40]. The net result of these arrested waves is much like that generated by an eddy field, namely an on-shore transport of dense waters that raises isopycnals over the slope. Before gateway deepening and the emergence of the

eastward slope current, this process was simply not present. The ability of a numerical model to capture such arrested wave is also resolution-dependent, as the wavelength of arrested waves gets smaller for decreasing flow speeds. In other words, the coarser the model grid gets, the lower is the ability to represent coastal upwelling by this process (requiring very high flow speeds) [41].

Although figure 5 shows that coastal upwelling in the AAB is resolution-dependent and therefore indicative of eddy-topography or wave-topography interactions, we cannot rule out a contribution from a bottom Ekman flow up the slope. And bottom Ekman dynamics can also take place in our 1° simulation. But as figures 3 and 4 clearly show, the flow near the bottom in this simulation is vanishingly small and isopycnal uplift over the continental slope is considerably underestimated. So the coarse-grained simulation has neither the small-scale nonlinear dynamics nor the required bottom flow needed to produce sufficient coastal upwelling in the AAB.

Finally, it is useful to keep in mind that the GM parameterisation used in the 1° simulation is designed to always flatten isopycnals, removing energy from the flow. As such, the scheme, which is the de facto industry standard eddy parameterisation in ocean climate simulation, will act to counter any original tendency for coastal upwelling, be it facilitated by nonlinear dynamics or bottom Ekman flow. So our 1° model simulation, as well as other non-eddying paleoclimate simulations used to study the EOT, are ill-equipped for capturing the central dynamics at play.

## 6. Summary and conclusions

Here we have provided the first dynamical explanation for key circulation changes in the Southern Ocean across the EOT. These results are documented in detail for the AAB, where high-resolution ocean model simulations are available. By comparing a hierarchy of simulations, from coarse-resolution eddy-parameterised configurations to high-resolution eddy-resolving simulations, we show that when mesoscale eddies are resolved the deepening of the Tasman Gateway leads to (i) the development of a proto-ACC which flows along the Antarctic continental slope through the AAB, and (ii) enhanced coastal upwelling in the AAB associated with this current. The upwelling is driven by either bottom Ekman transport beneath the boundary current or, as indicated by the highest-resolution simulations, eddy-topography or wave-topography interactions. We then show that none of this behaviour is seen in the coarse-resolution and eddy-parameterised simulations (such as reviewed by [6]), which explains why previous work does not show a strong effect of gateway deepening on ocean circulation. The generality of eddy-topography or wave-topography interactions to other sectors of the Antarctic margin, where circulation, slope geometry and bathymetric roughness differ, remains an open question.

The eddy-parameterised version of our model uses the GM parameterisation with a constant eddy transfer coefficient. This has the virtue of simplicity, whilst incorporating the considerable benefits of using GM. Even in this most basic of forms, GM is difficult to beat as an eddy parameterisation; it acts to reproduce the extraction of potential energy from sloping isopycnals by baroclinic instability, inducing an eddy-driven overturning and flattening isopycnals. Baroclinic instability is a ubiquitous process throughout the ocean that is thought to generate a large proportion of the ocean's mesoscale eddy field. The success of GM is evidenced by its tenure as the most widely-used eddy parameterisation in ocean modelling.

There are refinements of GM that use spatially/temporally varying transfer coefficients in an effort to produce a still more realistic ocean circulation. The simplest approaches use flow stability constraints to estimate the changing eddy coefficient [42]. More recently, considerable work has also been done aimed at using more complete descriptions of eddy energetics in parameterisations [5, 43–46]. These schemes have also been shown to be capable of reproducing emergent behaviour from eddying ocean models that are otherwise difficult to predict and reproduce [45]. Importantly, there is much evidence that eddy generation by baroclinic instability is suppressed over continental slopes, and eddy parameterisations that account for this effect are starting to emerge [47–49]. A coarse-resolution model applying such a topographically-sensitive GM scheme would not suppress Ekman-driven upwelling along the Antarctic continental slope to the extent that our current 1° model does. Nonetheless, even these schemes may err due to the fundamental design of GM itself, which is to always extract available potential energy from the flow and hence flatten isopycnals. The GM scheme simply misses the key process captured in the higher-resolution simulations, namely upwelling of dense waters. Ultimately, parameterization efforts need to be based on the idea that even though eddies are generated by the release of large-scale available potential or kinetic energy, what they actually transport is PV [50, 51]. And, as seen in this study, over continental slopes this can lead to uplifting rather than flattening of isopycnals. Early efforts along this

route of eddy PV mixing show promising results in a barotropic context [52]. But getting the energetics right for stratified flows is an ongoing challenge.

The other obvious way forward is to resolve eddies, as is becoming increasingly feasible due to recent model development leveraging modern GPU infrastructure efficiently [53], but despite these advancements, there will always be processes too small to be resolved directly, such as the intricate physics within the ocean's shallow planetary boundary layer. Consequently, accurate parameterisations of these small-scale processes will remain essential. This underscores the necessity for ongoing fundamental research into small-scale turbulent processes, including the development and refinement of their parameterisations. Additionally, rigorous testing of these parameterisations against observational data and turbulence-resolving simulations is crucial to ensure their reliability and accuracy.

In the future it will be exciting to reproduce the results from the ocean-only model here in a fully-coupled ESM in which eddy-topography interaction is resolved rather than parameterised, testing the influence of these ocean processes across the EOT on global climate during that part of Earth's past.

## Acknowledgments

This work was funded by the Australian Research Council Discovery Project (DP180102280) and the Australian Research Council Special Research Initiative for Antarctic Gateway Partnership (SR140300001). We acknowledge the Australian National Computational Infrastructure Merit Allocation Scheme projects and Australian Antarctic Division Grant AAS4567 for providing the computational resources. AK was funded by the Research Council of Norway grant KeyPOCP (328941) and PEI was partially funded by Research Council of Norway grant TopArctic (314826). IS was funded by the European Research Council under the European Community's Seventh Framework Program through ERC Starting Grant OceaNice (802835). The contributions of DRM were supported by the BIOPOLE National Capability Multicentre Round 2 funding from the Natural Environment Research Council (Grant No. NE/W004933/1).

## Data availability statement

No new data were created or analysed in this study.

## Author contributions

A Klocker 0000-0002-2038-7922
Conceptualization (equal), Data curation (equal), Formal analysis (equal), Funding acquisition (equal), Investigation (equal), Methodology (equal), Project administration (equal), Resources (equal), Supervision (equal), Validation (equal), Visualization (equal), Writing – original draft (equal), Writing – review & editing (equal)

P E Isachsen 0000-0003-1249-3052
Conceptualization (equal), Formal analysis (equal), Investigation (equal), Methodology (equal), Visualization (equal), Writing – original draft (equal), Writing – review & editing (equal)

D R Munday 0000-0003-1920-708X
Conceptualization (equal), Formal analysis (equal), Funding acquisition (equal), Investigation (equal), Methodology (equal), Writing – original draft (equal), Writing – review & editing (equal)

I Sauermilch
Conceptualization (equal), Data curation (equal), Formal analysis (equal), Investigation (equal), Methodology (equal), Visualization (equal), Writing – original draft (equal), Writing – review & editing (equal)

J M Whittaker 0000-0002-3170-3935
Conceptualization (equal), Funding acquisition (equal), Investigation (equal), Project administration (equal), Supervision (equal), Writing – original draft (equal), Writing – review & editing (equal)

## References


[1] Chelton D B, Schlax M G, Samelson R M and de Szoeke R A 2007 *Geophys. Res. Lett.* **34** L15606
[2] Chelton D B, Schlax M G and Samelson R M 2011 *Prog. Oceanogr.* **91** 167–216
[3] Jayne S R and Marotzke J 2002 *J. Phys. Oceanogr.* **32** 3328–45
[4] Mazloff M R, Heimbach P and Wunsch C 2010 *J. Phys. Oceanogr.* **40** 880–99
[5] Marshall J and Speer K 2012 *Nat. Geosci.* **5** 171–80
[6] Hutchinson D K *et al* 2021 *Clim. Past* **17** 269–315
[7] Sauermilch I, Whittaker J M, Klocker A, Munday D R, Hochmuth K, Bijl P K and LaCasce J H 2021 *Nat. Commun.* **12** 1–8
[8] Toumoulin A, Tardif D, Donnadieu Y, Licht A, Ladant J B, Kunzmann L and Dupont-Nivet G 2022 *Clim. Past* **18** 341–62
[9] Cramwinckel M J *et al* 2018 *Nature* **559** 382–6
[10] Lear C H, Elderfield H and Wilson P A 2000 *Science* **287** 269–72
[11] DeConto R and Pollard D 2003 *Nature* **421** 245–9
[12] Pearson P N, Foster G L and Wade B S 2009 *Nature* **461** 1110–3
[13] Anagnostou E, John E H, Edgar K M, Foster G L, Ridgwell A, Inglis G N, Pancost R D, Lunt D J and Pearson P N 2016 *Nature* **533** 380–4
[14] Kennett J P 1977 *J. Geophys. Res.* **82** 3843–60
[15] Scher H D, Whittaker J M, Williams S E, Latimer J C, Kordesch W E and Delaney M L 2015 *Nature* **523** 580–3
[16] Pollard D, Kump L R and Zachos J C 2013 *Glob. Planet. Change* **111** 258–67
[17] Armstrong McKay D I, Tyrrell T and Wilson P A 2016 *Paleoceanography* **31** 311–29
[18] Hochmuth K, Whittaker J M, Sauermilch I, Klocker A, Gohl K and LaCasce J H 2022 *Nat. Commun.* **13** 1–10
[19] Evangelinos D *et al* 2024 *Nat. Geosci.* **17** 165–70
[20] Hutchinson D K, Coxall H K, O'Regan M, Nilsson J, Caballero R and de Boer A M 2019 *Nat. Commun.* **10** 3797
[21] Straume E O, Nummelin A, Gaina C and Nisancioglu K H 2022 *Proc. Natl Acad. Sci.* **119** e2115346119
[22] Gaina C, Jakobsson M, Straume E O, Timmermans M L, Boggild K, Bünz S, Schlindwein V and Døssing A 2025 *Nat. Rev. Earth Environ.* **6** 211–27
[23] Xing Q, Munday D, Klocker A, Sauermilch I and Whittaker J 2022 *Clim. Past* **18** 2669–93
[24] Xing Q, Klocker A, Munday D and Whittaker J 2023 *Geophys. Res. Lett.* **50** 1–11
[25] Hochmuth K, Gohl K, Leitchenkov G, Sauermilch I, Whittaker J M, Uenzelmann-Neben G, Davy B and De Santis L 2020 *Geochemistry, Geophys., Geosystems* **21** 1–28
[26] Styles A F, Bell M J and Marshall D P 2023 *J. Geophys. Res.: Oceans* **128** e2023JC019711
[27] Marshall J, Adcroft A J, Hill C, Perelman L and Heisey C 1997 *J. Geophys. Res.* **102** 5753–66
[28] Gent P R and McWilliams J C 1990 *J. Phys. Oceanogr.* **20** 150–5
[29] Gent P R, Willebrand J, McDougall T J and McWilliams J C 1995 *J. Phys. Oceanogr.* **25** 463–74
[30] Hutchinson D K, De Boer A M, Coxall H K, Caballero R, Nilsson J and Baatsen M 2018 *Clim. Past* **14** 789–810
[31] Thompson A F, Speer K G and Schulze Chretien L M 2020 *Geophys. Res. Lett.* **47** e2020GL087802
[32] Nøst O A and Isachsen P E 2003 *J. Mar. Res.* **61** 175–210
[33] Wang Y and Stewart A L 2018 *Ocean Modelling* **121** 1–18
[34] Gill A, Green J and Simmons A 1974 *Deep Sea Res.* **21** 499–528
[35] Marshall J and Radko T 2003 *J. Phys. Oceanogr.* **33** 2341–54
[36] Holloway G 1987 *J. Fluid Mech.* **184** 463–76
[37] Klocker A 2018 *Sci. Adv.* **4** eaao4719
[38] Bachman S and Klocker A 2020 *J. Phys. Oceanogr.* **50** 2873–83
[39] Charney J G and Eliassen A 1949 *Tellus* **1** 38–54
[40] Haidvogel D B and Brink K H 1986 *J. Phys. Oceanogr.* **16** 2159–71
[41] LaCasce J H, Nøst O A and Isachsen P E 2008 *J. Phys. Oceanogr.* **38** 517–526
[42] Visbeck M, Marshall J, Haine T and Spall M 1997 *J. Phys. Oceanogr.* **27** 381–402
[43] Cessi P 2008 *J. Phys. Oceanogr.* **38** 1807–19
[44] Eden C and Greatbach R J 2008 *Ocean Modell.* **20** 223–39
[45] Mak J, Marshall D P, Maddison J R and Bachman S D 2017 *Ocean Modelling* **112** 125–38
[46] Mak J, Maddison J R, Marshall D P and Munday D R 2018 *J. Phys. Oceanogr.* **48** 2363–82
[47] Wang Y and Stewart A L 2020 *Ocean Modelling* **147** 101579
[48] Wei H and Wang Y 2021 *J. Adv. Model. Earth Syst.* **13** 1–40
[49] Nummelin A and Isachsen P E 2024 *J. Adv. Model. Earth Syst.* **16** e2023MS003806
[50] Adcock S T and Marshall D P 2000 *J. Phys. Oceanogr.* **30** 3223–38 (available at: https://journals.ametsoc.org/view/journals/phoc/30/12/1520-0485_2000_030_3223_ibgeat_2.0.co_2.xml)
[51] Marshall D P and Adcroft A J 2010 *Ocean Modelling* **32** 188–204
[52] Eaves R E, Maddison J R, Marshall D P and Waterman S 2025 *J. Phys. Oceanogr.* **55** 573–91
[53] Silvestri S, Wagner G L, Constantinou N C, Hill C N, Campin J M, Souza A N, Bishnu S, Churavy V, Marshall J and Ferrari R 2025 *J. Adv. Model. Earth Syst.* **17** e2024MS004465